The keratin-filament cycle of assembly and disassembly

Anne Kölsch[1],*, Reinhard Windoffer[1],*,‡, Thomas Würflinger[2], Til Aach[2] and Rudolf E. Leube[1],‡

[1]Institute of Molecular and Cellular Anatomy, RWTH Aachen University, 52074 Aachen, Germany
[2]Institute of Imaging and Computer Vision, RWTH Aachen University, 52056 Aachen, Germany
*These authors contributed equally to this work
‡Authors for correspondence (rwindoffer@ukaachen.de; rleube@ukaachen.de)

Summary

Continuous and regulated remodelling of the cytoskeleton is crucial for many basic cell functions. In contrast to actin filaments and microtubules, it is not understood how this is accomplished for the third major cytoskeletal filament system, which consists of intermediate-filament polypeptides. Using time-lapse fluorescence microscopy of living interphase cells, in combination with photobleaching, photoactivation and quantitative fluorescence measurements, we observed that epithelial keratin intermediate filaments constantly release non-filamentous subunits, which are reused in the cell periphery for filament assembly. This cycle is independent of protein biosynthesis. The different stages of the cycle occur in defined cellular subdomains: assembly takes place in the cell periphery and newly formed filaments are constantly transported toward the perinuclear region while disassembly occurs, giving rise to diffusible subunits for another round of peripheral assembly. Remaining juxtanuclear filaments stabilize and encage the nucleus. Our data suggest that the keratin-filament cycle of assembly and disassembly is a major mechanism of intermediate-filament network plasticity, allowing rapid adaptation to specific requirements, notably in migrating cells.

Key words: Cytokeratin, Network dynamics, Live-cell imaging

Introduction

The cytoplasmic cytoskeleton of mammalian cells is composed of three major filament networks – actin filaments, microtubules and intermediate filaments (IFs). This scaffolding is not simply a static system conferring stability on cells, but is highly dynamic and capable of rapid reorganization in response to various extracellular and intracellular stimuli. Adjustment of actin filaments and microtubules is accomplished through differential regulation of polymerization at either end, depending on the availability of nucleoside-triphosphate-bound soluble subunits and regulatory factors. One prominent mechanism of filament remodelling is treadmilling, which exploits the structural asymmetry of filament ends (Amann and Pollard, 2000; Margolis and Wilson, 1981; Pollard et al., 2000). Thus, subunits dissociate from the minus end and are added to the plus end. IFs are profoundly different from actin filaments and microtubules because they lack polarity as a result of the symmetric composition of their tetrameric subunits. Furthermore, spontaneous self-assembly of tetramers into unit-length filaments (ULFs), followed by compaction and longitudinal annealing, occurs – at least in vitro – without nucleoside triphosphates and additional cofactors (Herrmann et al., 2007; Kim and Coulombe, 2007). How these in vitro observations relate to the in vivo situation and how assembly is regulated is not understood.

IFs are ubiquitous cytoskeletal components that are particularly abundant in epithelial cells. Epithelial IFs are composed of desmosome-anchored keratins, providing a mechanically resilient, complex scaffold (Sivaramakrishnan et al., 2008) that responds quickly to various stimuli through specific structural adaptations. Metabolic, thermal and mechanical stress therefore results in considerable keratin IF (KF) reorganization (Magin et al., 2007;

Pekny and Lane, 2007). Recent observations further revealed that the keratin system affects many basic cellular processes, such as growth, proliferation, organelle transport, malignant transformation and stress response, further accentuating the dynamic properties of the keratin network (Magin et al., 2007). Thus, interference with KF dynamics in human disease and transgenic mice leads to reduced resilience of epithelia to mechanical and other challenges with deleterious functional consequences (Arin, 2009; Vijayaraj et al., 2007). For this reason, elucidating the still-unresolved molecular mechanisms of KF-network biogenesis and turnover is a pressing issue.

At present, two conceptually different hypotheses are being discussed to explain IF assembly in living cells. The first model, which was recently termed dynamic co-translation, stresses the integration of newly synthesized IF polypeptides at multiple sites throughout the entire network (Chang et al., 2006; Goldman et al., 2008). An alternative model suggests that keratin particles are preferentially generated at distinct loci in the cell periphery, subsequently integrating into the peripheral keratin cytoskeleton (Windoffer et al., 2006; Windoffer et al., 2004). Although both scenarios provide concepts explaining how the network 'grows', they do not address the problem of how the fully assembled network changes over time. This is crucial for adaptation to varying environmental conditions, for example, during development and under mechanical stress.

The goal of our study was to fill the existing gaps in these two hypotheses and to evaluate their contribution to KF-network dynamics. Using live-cell imaging, we discovered a protein-biosynthesis-independent multistep disassembly and assembly cycle that is continuously active and allows rapid keratin-network adaptation, for instance in migrating cells.

Results

Keratin-filament network precursor formation occurs preferentially in lamellipodia of migrating cells and persists in the presence of protein biosynthesis inhibitors

It was observed by time-lapse fluorescence recording of cell lines producing fluorescent epithelial KFs that KF formation occurs preferentially at free cell edges and adjoining cell borders of stationary cells (Kolsch et al., 2009; Windoffer et al., 2004). After scratch wounding, abundant KF precursors (KFPs) were seen at the leading edge of approaching cells, thereby extending the IF cytoskeleton towards the gap (Fig. 1A; supplementary material Movie 1). This was also noted in single migrating cells (Fig. 1B-E; supplementary material Movie 2). KFPs grow by elongation and fusion until integration into the peripheral KF network (for details, see Windoffer et al., 2004; Woll et al., 2005).

Considering the abundance of keratin particles in the cell periphery of wounded and migrating cells, we wanted to know whether protein biosynthesis is sufficient to account for keratin assembly, as predicted by the dynamic co-translation model (Chang et al., 2006). Treatment with the translation inhibitors cycloheximide and puromycin, however, did not prevent KFP formation (Fig. 2; supplementary material Movies 3 and 4). KFPs can therefore assemble from a pre-existing keratin pool that is either of significant size or continuously replenished.

Keratin filaments translocate continuously toward the nucleus

Newly formed KFPs are continuously transported toward the nucleus, relying primarily on intact actin filaments (Kolsch et al.,

2009; Woll et al., 2005). To further track KFs after integration into the peripheral network, image-processing algorithms were developed and applied to motility analyses. First, global cellular movement was compensated for. Then, the medians of the translation vectors were computed for each grid point over time, assuming long-term local stability of keratin movement. This revealed coordinated and continuous centripetal keratin movement all the way to the nucleus at an average speed of ~250 nm/minute, with local heterogeneities between 100 and 600 nm/minutes (Fig. 3; supplementary material Movie 5). The motion stopped upon reaching the juxtanuclear region.

Inward-moving keratin filaments disassemble into non-filamentous subunits

Given the movement of the entire keratin system toward the nucleus, one would expect an incremental build up of keratin fluorescence near the nucleus; this is obviously not the case. To test the hypothesis that KFs disassemble, the fluorescence of selected KF subsets was monitored (Fig. 4; supplementary material Movies 6 and 7). First, regions of interest (ROIs) were defined between prominent peripheral KF bundles. The enclosed KFs translocated continuously towards the nucleus while fusing, generating fewer and thicker bundles (Fig. 4A-F; supplementary material Movie 6). As a result, the ROI size shrank (Fig. 4H). Fluorescence quantification revealed gradual loss that was fast during the first 1-2 hours (~40% loss/hour), affecting the younger peripheral filaments, and slow later (<10% loss/hour), affecting the older thickened filament bundles (Fig. 4I), which eventually stabilize to form the juxtanuclear static cage. This difference is
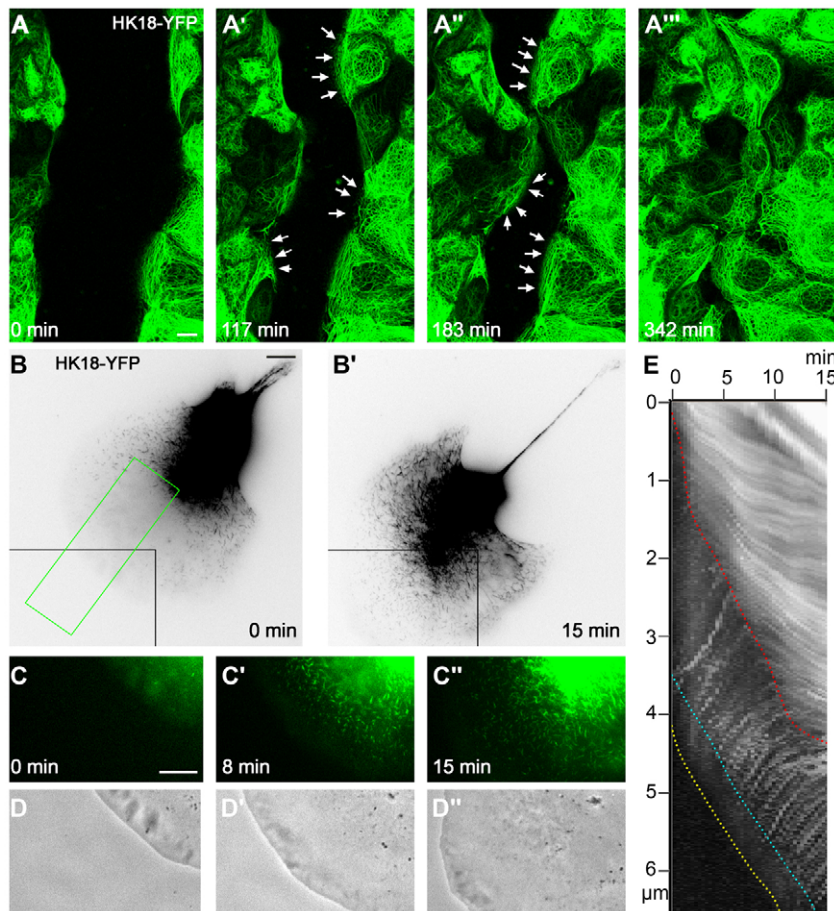
Fig. 1. KFPs are predominantly formed at the leading edge of migrating cells. (A-A‴) A wound was induced by scratching a confluent monolayer of mammary-epithelium-derived EK18-1 cells that produce fluorescent HK18-YFP with a microinjection needle. Fluorescence images were then recorded until the wound had closed. Selected images are shown in A-A‴, demonstrating the continuous and collective convergence of both edges. Multiple KFPs were observed in lamellipodial protrusions of the approaching cells, which can be best appreciated in accompanying supplementary material Movie 1, and are marked by arrows in selected cells. (**B-C″**) Fluorescence images (inverse representation) are shown of a migrating EK18-1 cell with a large lamellipodium containing multiple KFPs that are depicted at higher resolution in C-C″. Corresponding phase-contrast images are shown in **D-D″**. The images are taken from a 15 minute time-lapse recording of fluorescence and phase contrast (see supplementary material Movie 2). (**E**) The kymogram was prepared from supplementary material Movie 2, corresponding to the boxed green area in B. It shows the appearance of multiple KFPs in the lamellipodium in proximity to the plasma membrane (yellow line). The blue line depicts the position of first KFP detection. The subsequent inward-directed movement of KFPs until integration into the peripheral KF network (red line) occurs at similar speed in each instance (slope of line). Scale bars: 10 μm.

best appreciated when the substantial initial fluorescence loss in the blue, green and pink ROIs is compared with the lower initial loss in the red ROI, which was already more central when measurements began (Fig. 4). The apparent fluorescence loss is not caused by bleaching, because overall cellular fluorescence did not decrease. Furthermore, degradation can also be excluded as a major contributing factor, because the fluorescence decrease in entire cells was less than 5% per hour in the presence of puromycin (n=4).

To directly monitor disassembly of selected filament bundles, short filament pieces were 'isolated' by bleaching the surrounding areas (Fig. 4J-N; supplementary material Movie 7). These experiments showed that fluorescence decreased continuously and was not associated with filament fragmentation (i.e. particle formation). We therefore conclude that KFs disintegrate on their way to the nucleus by the release of small, non-filamentous oligomers that cannot be resolved as single particles, but appear as a diffuse weak signal throughout the cytoplasm.

Cells contain a diffusible pool of keratins

To examine the nature of the non-filamentous pool of disassembled KFs, fluorescence recovery after photobleaching (FRAP) analyses were performed. Filament-free regions were selected within bleached areas to measure the mobile fraction of non-filamentous keratins. The mobile fraction was 52.2±12.4% in PK18-5 cells (n=5). The diffusion coefficient of this mobile fraction was determined to be 0.88±0.08 μm^2/second for human keratin 18 (HK18)-YFP fusion protein (n=9). Furthermore, the diffusion coefficient was not significantly altered in the presence of cytochalasin and nocodazole [1.06±0.31 μm^2/second for HK18-YFP (n=8); P=0.1052]. In control experiments, the diffusion coefficient for YFP alone was 27.10±7.15 μm^2/second (n=20),

which is in close agreement with the values for GFP measured by fluorescence correlation spectroscopy (FCS) (Dross et al., 2009). These findings reveal the existence of a mobile and diffusible cytoplasmic keratin pool whose precise composition and multimerization stage, however, still need to be determined by more sensitive and accurate methods, such as FCS.

Disassembled keratin-filament subunits are reutilized for peripheral keratin-filament assembly

To demonstrate that assembling peripheral KFs are made from material that is derived from disassembled KFs, peripheral cytoplasmic zones of HK18-YFP-producing cells were bleached (Fig. 5A). The mean fluorescence recovery in the peripheral cytoplasm was 72±24% after 15 minutes (n=4). During the same time interval, 7.3±2.8% of the fluorescence was lost in the central, non-bleached region, presumably due to translocation of non-filamentous material to the cell periphery.

Next, an entire cell half was bleached (Fig. 5B). The appearance of fluorescence predominantly in the periphery of the bleached half and its subsequent movement to the cell interior are clearly seen in supplementary material Movie 8. Fluorescence intensities were measured within and outside of the bleached areas, and also in the neighbouring unbleached control cells. As expected, fluorescence increased gradually in the bleached red ROI, with ~60% recovery after 1 hour (Fig. 5B). The recovery rate in this ROI is slower than that determined in the previous experiment (Fig. 5A), because of its more central location and the lower availability of material due to the much more extended bleaching. Remarkably, fluorescence in the unbleached part of the cell decreased during the 60 minute observation period and approached levels similar to those measured in the bleached area, thus providing evidence of continuing KF-network turnover. In comparison, the
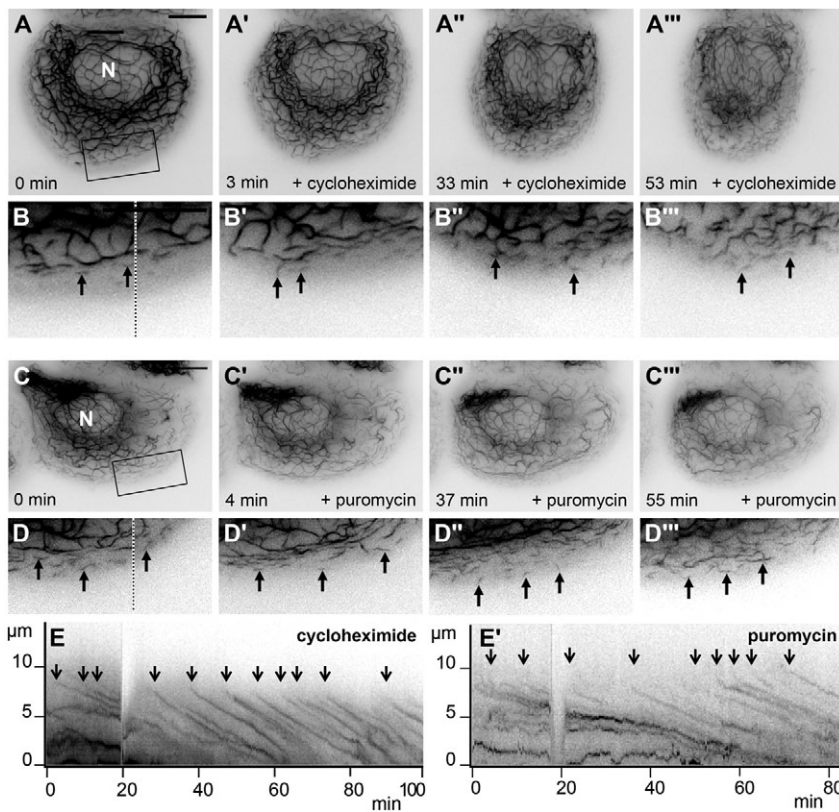
Fig. 2. KFP formation persists in the presence of protein biosynthesis inhibitors. (A-D‴) Hepatocellular-carcinoma-derived PLC cells of clone PK18-5 stably producing keratin chimera HK18-YFP were treated at 20 minutes with the translation inhibitors cycloheximide (17 μM; A-A‴; high magnifications of boxed region in B-B‴) or puromycin (1 μg/ml; C-C‴; high magnifications of boxed region in D-D‴). The images were taken from supplementary material Movies 3 and 4. Note that KFP formation and KFP integration into the KF network are not prevented in either instance. Arrows in B-B‴ and D-D‴ depict newly appearing KFPs, as determined from the corresponding movies. (**E,E′**) Kymograms were prepared from the fluorescence recorded along the dashed lines in B and D, respectively, which further demonstrates ongoing KFP formation (marked by arrows) and inward-directed movement after drug application (addition of drugs at 20 minutes). N, nucleus. Scale bars: 10 μm.
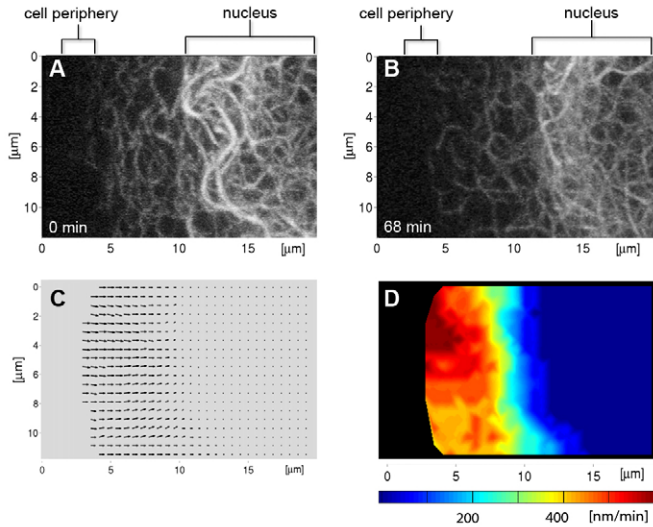
Fig. 3. The KF network translocates continuously towards the nucleus.
(**A,B**) Fluorescence micrographs showing a section of a PK18-5 cell (projected images of 22 focal planes) at time points 0 and 68 minutes (cell periphery at left, nucleus at right) observed by time-lapse imaging (60 second intervals; see corresponding supplementary material Movie 5). (**C**) Vector visualization of the direction and speed of KFs in this cell segment. Z-axis projections of all volume were superimposed on grids of overlapping ROIs at 10-pixel spacing. Between consecutive frames, each ROI was rigidly registered by the SSD criterion using a weighted window to emphasize central parts. Assuming long-term local stability of keratin movement, medians of the translocation vectors were computed for each grid point over time. (**D**) Velocities from C depicted in pseudo-colour representation.

fluorescence intensity in a corresponding ROI of the adjacent control cell remained almost the same, except for a slight increase that is most probably due to de novo protein biosynthesis (see also Fig. 4I).

Photoactivation experiments were designed to obtain positive proof that filament-bound keratin molecules are released and used for reassembly of new filaments without the need for de novo biosynthesis. After photoactivating human keratin 8 (HK8) hybrids in entire cell halves, new fluorescence appeared in the non-activated parts, the source of which can only be the filament-bound photoactivated molecules from the other cell half (Fig. 5C-D). Within 4 hours, an almost even distribution was noted throughout the cytoplasm (not shown). This is in rough agreement with the bleaching experiments, in which complete exchange of the KF network was observed within 4 hours (supplementary material Movie 8) (data not shown). Furthermore, photoactivated filaments concentrated around the nucleus, whereas inward-moving filaments re-appeared in the cell periphery (see Fig. 5D for quantifications). In support of this, photoactivating only perinuclear filaments resulted in the 'spreading' of fluorescence to the cell periphery (Fig. 5E-F).

Discussion

Combining the current observations with previous reports on keratin dynamics, key steps of the KF assembly and disassembly cycle have begun to emerge.

Nucleation

Nucleation of KFPs occurs preferentially in the cell periphery (Fig. 1 and Fig. 5B; supplementary material Movies 1, 2, 8)
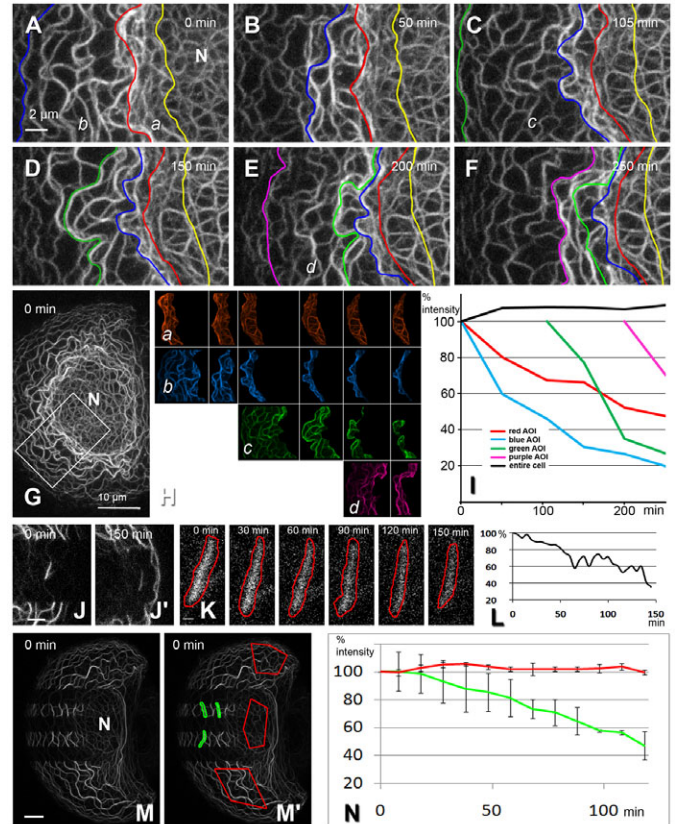
Fig. 4. Inward-moving KFs disassemble into non-filamentous subunits.
(**A-G**) Images taken from a 250 minute time-lapse recording of HK18 fluorescence in a PK18-5 cell (overview shown in G, with the boxed area delineating a region shown at high magnification in A-F). The confocal 4D data sets were recorded at 12 bit (recording interval 5 minutes; 11 planes each) for 250 minutes (supplementary material Movie 6). The coloured lines in A-F represent borders of ROIs that were defined in the outer part of the KF network between characteristic KF bundles. The borders were traced manually in the projection images of each time point of the recording to ensure proper delineation. The individual ROIs are depicted in (**Ha-d**). Note that all ROIs moved from the cell periphery towards the nucleus (N), that is, from left to right, during the recording. The size of each ROI decreased continuously over time (H). In addition, the relative fluorescence intensity in each ROI (or AOI) decreased over time, with a fast component in the beginning and a slow component later on (**I**; same colour code as in H). The black line in I shows the fluorescence intensity of the entire cell over time. Scale bars: 2 μm (A), 10 μm (G). (**J-L**) Projected fluorescence images (19 planes) and diagram from a time-lapse series of a PK18-5 cell in which a single fluorescent KF fragment was 'isolated' by bleaching the surrounding KFs. The nucleus (outside the depicted area) is to the left, the cell periphery to the right. The isolated KF fragment is shown at higher magnification at different time points in K. The red line depicts the border of the manually assigned ROIs, the intensities of which are plotted in L over time, revealing continuous fluorescence loss. Scale bars: 2 μm (J), 0.5 μm (K). (**M-N**) Projected images (25 planes) at time point 0 minutes and a diagram derived from a subsequent time-lapse series (supplementary material Movie 7). The PK18-5 cell (N, nucleus) was bleached in such a way that fluorescent filament 'fragments' remained in two sectors. This allowed measurement of fluorescence in these singled out KFs. ROIs that are shown in green in M′ were manually adjusted at each time point. The fluorescence of these mobile ROIs was measured over time and compared to the fluorescence in fixed ROIs (red in M′) within unbleached parts of the cell. The results for the three mobile and fixed ROIs are summarized in the graph in N. Note the fluorescence decrease in the green ROIs due to filament disassembly, whereas it stays constant in the red ROIs, where fluorescence loss from filament disassembly is compensated by incoming new filaments. Scale bar: 10 μm (M).
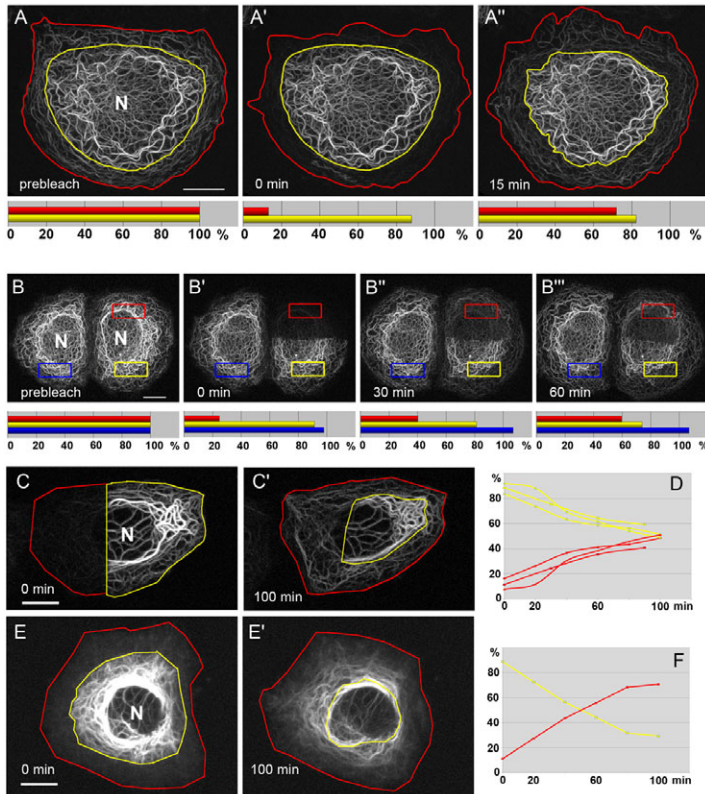
Fig. 5. KFs disassemble to support KF assembly in the peripheral cytoplasm. (A-B‴) Two representative FRAP experiments are depicted that were performed in PK18-5 cells producing HK18-YFP. (A) The peripheral network was bleached throughout the entire circumference in a zone extending ~5 μm from the plasma membrane to the cell interior (area between red and yellow lines). The shape of the bleached and non-bleached areas was adjusted by hand to account for cellular shape shifts. Within 15 minutes, considerable fluorescence recovery was observed in the periphery (compare A′ and A″). The histograms below summarize the results of fluorescence quantification in this and three similarly treated cells. The red bars correspond to the average fluorescence recovery in the cell periphery, whereas the yellow bars correspond to the average fluorescence measured in the central cytoplasm. (B) Half of a PK18-5 cell was bleached. Fluorescence recovery measured in the boxed ROI (red), which encompasses mainly central filaments, was ~60% within 60 minutes (red bars in histograms below). By contrast, filaments in the corresponding unbleached ROI (yellow box) decreased within the same time period (yellow bars). For comparison, an ROI in a neighbouring cell that was not bleached at all (blue box) shows slight increase in fluorescence, possibly due to de novo synthesis (blue bars). Corresponding supplementary material Movie 8 presents an image series of 3D reconstructions of the altering fluorescence patterns. **(C-F)** Photoactivatable GFP fused to keratin 8 (HK8-paGFP) was expressed in PLC cells. HK8-paGFP fluorescence was activated with UV light (405 nm) in different cell regions. Subsequently, fluorescence was monitored at 488 nm by time-lapse fluorescence microscopy. Note the appearance of fluorescence in the non-activated parts of the cells (C′,E′). In addition, fluorescence concentrated in the perinuclear domain, whereas peripheral fluorescence was generated from new filament formation. Quantification of fluorescence (in percent of total fluorescence) shows gradual depletion of photoactivated regions (yellow) and simultaneous fluorescence increase in non-activated areas (red). D, n=3 and F (derived from E,E′). N, nucleus. Scale bars: 10 μm.

(Windoffer et al., 2006; Windoffer et al., 2004; Yoon et al., 2001). Cells with increased KF-network reorganization, such as migrating cells, show a considerable increase in KFP formation (Fig. 1) (Windoffer et al., 2006; Woll et al., 2005). Focal adhesions are important regulators of keratin nucleation (Windoffer et al., 2006) by direct and/or indirect molecular association [(Steinbock et al., 2000); for other IFs, see the following references (Kreis et al., 2005; Nikolic et al., 1996; Spurny et al., 2008; Steinbock et al., 2000; Sun et al., 2008a; Sun et al., 2008b; Tsuruta and Jones, 2003)] and/or by signalling (e.g. Omary et al., 1998; Woll et al., 2007).

Elongation
KFPs elongate by continuous integration of soluble oligomers at either end and mutual end-on fusion (Fig. 1B-D) (Windoffer et al., 2006; Windoffer et al., 2004; Woll et al., 2005) [for other IFs, see the following references (Colakoglu and Brown, 2009; Kirmse et al., 2007)].

Integration
End-on integration of KFPs into the peripheral KF network terminates elongation and thereby introduces branch points into the filament network (Windoffer et al., 2006; Windoffer et al., 2004; Woll et al., 2005).

Bundling
The thickness of the KF bundles increases towards the nucleus because of the lateral association of filament bundles (Figs 3-5; supplementary material Movies 5, 6 and 8). Bundling is regulated by IF-associated polypeptides (Listwan and Rothnagel, 2004) and intrinsic properties of KFs (Lee and Coulombe, 2009).

Vectorial transport
An intact actin-filament system is required for inward-directed KFP transport. The actin retrograde flow and ruffling activity (Small and Resch, 2005) might provide the driving force for centripetal KF movement (Kolsch et al., 2009; Windoffer et al., 2006; Windoffer and Leube, 2001; Woll et al., 2005). Microtubules might also be needed, especially for the subsequent inward motion of the entire network (for a review, see Helfand et al., 2004).

Disassembly
Inward-moving KFs dissolve without the appearance of distinct particles (Fig. 4) either by degradation of KF polypeptides and/or by disassembly into reusable non-filamentous subunits. Although keratin ubiquitylation has been implicated in KF-network turnover (Ku and Omary, 2000) and occurs in stress and disease (Jaitovich et al., 2008; Zatloukal et al., 2007), the second mechanism appears to be the major mode because pre-existing filaments are the source of protein-biosynthesis-independent peripheral filament formation. Of note, the static juxtanuclear filaments are quite stable, as is the case for desmosome-anchored KFs (Strnad et al., 2002).

Diffusion
A rather small though significant mobile fraction of fluorescent keratins with a fast recovery rate was identified in this study. This diffusible keratin pool corresponds, at least in part, to the detergent-soluble pool, which consists primarily of tetramers and also higher order oligomers (Bachant and Klymkowsky, 1996; Chou et al., 1993; Soellner et al., 1985), as indicated by a diffusion coefficient that was significantly lower than that of YFP alone. The identification of diffusing keratins shows that active transport machinery is not needed to deliver disassembled keratins to the

cell periphery for KF reassembly. This is also supported by the finding that KFP formation persists, although at reduced levels, in the presence of actin filament and microtubule disruptors (Kolsch et al., 2009; Woll et al., 2005). The soluble pool is also available for lateral exchange into existing filaments (Miller et al., 1991), which might explain the slight recovery of bleached filaments in our recordings (e.g. supplementary material Movies 7 and 8).

The revealed keratin cycle is different from dynamic co-translation (Chang et al., 2006), because it is independent of protein biosynthesis, does not require microtubules and occurs in a spatially defined manner. Our data suggest that the turnover cycle accounts for the vast majority of newly formed filaments. In contrast to the estimated ~25% hourly turnover rate of the keratin cycle, biosynthesis appears to be less than 5% per hour, as inferred from the overall fluorescence increase (e.g. Fig. 5B; Fig. 3N; data not shown). It will be of interest to determine the different contributions of the keratin cycle and dynamic co-translation mechanisms to network plasticity in relation to IF type, cell specialization and specific situation.

The keratin cycle maintains a stationary network at steady state. Preferential assembly at the leading edge of migrating cells leads to an imbalance and subsequent extension of the network towards the lamellipodium. The self-sufficient keratin cycle can be accelerated or slowed by external factors, depending on specific requirements. In support of this, both assembly and disassembly of wild-type and mutant keratins are slowed by p38 mitogen-activated protein kinase inhibitors (Woll et al., 2007). This observation indicates the presence of a basic mechanism whereby signalling affects network reorganization. It exemplifies how keratin-network cycling can be modulated by various types of stress, most notably mechanical stress. Furthermore, regional regulation of the keratin cycle facilitates network restructuring in specific cell topologies. This is needed, for example, in wounded tissues, in which migrating cells not only have to maintain a functional transcellular network but also need to modulate their network architecture during wound closure.

Materials and Methods

DNA cloning
Preparation of expression vectors pHK18-YFP and pHK8-CFP, which contain cDNA encoding fusion proteins HK18-YFP and HK8-CFP, respectively, has been described previously (Strnad et al., 2002; Windoffer and Leube, 2004). Plasmid clone paGFP-N1, encompassing a CMV-promoter-driven cDNA encoding photoactivatable green fluorescent protein (paGFP), was kindly provided by George Patterson (NIH, Bethesda, MD) (Patterson and Lippincott-Schwartz, 2002). To prepare cDNA encoding HK8-paGFP, HK8 cDNA was excised with *Bam*HI and *Eco*RI from plasmid pHK8-CFP and inserted into the paGFP-N1 vector.

Cell-culture experiments and manipulation
The human hepatocellular-carcinoma-derived epithelial cell line PLC and the stable HK18-YFP-producing subclone PK18-5 were described previously (Strnad et al., 2002). Spontaneously immortalized mouse mammary epithelial cells of line EpH4 and stable transfectants synthesizing HK18-YFP have been presented elsewhere (Kolsch et al., 2009).

For assessment of drug-induced keratin alterations, cells were seeded in glass-bottom Petri dishes (MatTek) and treated with 17 µM cycloheximide (Windoffer et al., 2000) (Sigma) or 1-2 µg/ml puromycin (Sigma).

Scratch-wounding assays were performed in completely confluent cell monolayers producing homogenously labelled KF networks using a microinjection needle. KF-network reorganization during wound closure was monitored by recording time-lapse fluorescence images.

Live-cell imaging
Cells were imaged by epifluorescence and confocal laser-scanning microscopy as described (Windoffer and Leube, 2004). Conversion of paGFP was done by irradiation with five successive scans of 405 nm light at 100% laser intensity.

FRAP experiments
Two types of FRAP experiments were performed to either characterize fast processes concerning non-filamentous keratins or examine the comparatively slow KF dynamics.

To determine the mobile fraction of non-filamentous keratins, a Zeiss 710 confocal laser-scanning microscope was used. Square regions of ~8×15 µm were bleached in the peripheral cytoplasm using the 488 nm laser at high intensity. Twenty frames were recorded within the next 10-20 seconds. Within the respective bleached regions, completely filament-free irregularly shaped ROIs of 1-2 µm width were chosen and fluorescence recovery in these ROIs was analyzed with the help of Zeiss Zen software.

To determine diffusion coefficients, 5 µm diameter ROIs were bleached in the cell periphery and recovery was measured at 0.668 second intervals for 30 seconds. The recovery curves were fitted according to the following equation (Ellenberg et al., 1997):

$$I_{(t)} = I_{(final)}(1 - (w^2(w^2 + 4\pi Dt)^{-1})^{1/2}),$$

where $I_{(t)}$ is intensity as a function of time, w is the width of ROI (diameter), D is the diffusion constant and t is time. As negative control, cells were fixed with methanol/acetone to demonstrate loss of fluorescence recovery. To exclude active transport, cells were treated with 25 µM cytochalasin D and 75 µM nocodazole (both from Sigma) 30 minutes prior to bleaching. For statistical evaluation, a two-tailed t-test was performed.

To characterize the slower KF dynamics, a Leica TCS SP5 confocal laser-scanning microscope was employed. Complete fluorescence was measured in single cells and stacks of images containing 4096 grey values (12 bit) were recorded with the 488 nm laser excitation line prior to bleaching. Step size was between 300 and 500 nm. For bleaching, the 488 nm laser line was applied to different ROIs at high intensity until the fluorescence was below 10% of the pre-bleach level. Starting directly after bleaching, stacks were recorded at regular intervals using the same parameters as for pre-bleach image recording.

Image generation from 3D stacks and quantification of fluorescence
To measure fluorescence intensities in 3D stacks of time series, maximum intensity projections were first generated using ImageProPlus software (Media Cybernetics). The projected images were used for preparing figures and movies. For quantification, ROIs were selected from these projected images. Then, the sum of the grey values was determined in the corresponding ROIs of each image of the z-stack. The values determined for the ROIs in all planes of a stack were then added to calculate the complete 3D fluorescence intensity of a ROI. For comparison of ROI intensities at different time points, it was often necessary to re-define ROIs to account for shifting, size changes and deformation. To correct measurements for background noise, the mean of the grey level per pixel was measured in cell-free regions and subtracted from the grey values determined for pixels measured inside the ROI. Measurements were analyzed with the help of Excel spreadsheets.

Kymograms
To represent movement of KFPs, kymograms were prepared from time-lapse fluorescence recordings. Regions were selected extending from the cell edge to the central cytoplasm. Amira software (Visage Imaging) was used to project the enclosed fluorescence and plot it over time.

Tracking of filaments
Confocal 4D data sets were recorded at 12 bit in cells producing fluorescent keratins. Projections of each time point were used for tracking. ROIs containing a distinct population of filaments were manually defined and Amira software was used to adapt the edges of the chosen ROIs to altered shape in the following frames by visual inspection. From selected time points, the fluorescence intensity of all ROIs was determined by adding their grey values in all 11 planes using ImagePro Plus macros.

In some instances, global cellular movement was compensated by an image-intensity-based registration method (Würflinger et al., 2008) using the normalised sum of squared intensity differences (SSDs). Robustness was increased by embedding the registration in a multiscale Gaussian pyramid framework. Visual assessment of the results revealed no misalignments. Based on the aligned image series, analyses could be restricted to intracellular keratin motion. A z-axis projection of each volume was superimposed by a grid of ROIs at 10-pixel spacing. The overlapping ROIs were of 41-pixel width. Each ROI was rigidly registered to the previous frame by SSD criterion using an exhaustive search for translations of ±20 pixels. SSD was modified by a weighted window function on the ROIs, which dropped linearly from the centre to zero. Thus, the non-rigid character of the data was accounted for and enough structural information was captured by the ROIs, similarly to the work of Wilkie and Vrscay (Wilkie and Vrscay, 2005). Assuming long-term local stability of the keratin flow, the medians of the translation vectors were computed for each grid point over time.

Supplementary material available online at
http://jcs.biologists.org/cgi/content/full/123/13/2266/DC1

References

Amann, K. J. and Pollard, T. D. (2000). Cellular regulation of actin network assembly. *Curr. Biol.* **10**, R728-R730.

Arin, M. J. (2009). The molecular basis of human keratin disorders. *Hum. Genet.* **125**, 355-373.

Bachant, J. B. and Klymkowsky, M. W. (1996). A nontetrameric species is the major soluble form of keratin in Xenopus oocytes and rabbit reticulocyte lysates. *J. Cell Biol.* **132**, 153-165.

Chang, L., Shav-Tal, Y., Trcek, T., Singer, R. H. and Goldman, R. D. (2006). Assembling an intermediate filament network by dynamic cotranslation. *J. Cell Biol.* **172**, 747-758.

Chou, C. F., Riopel, C. L., Rott, L. S. and Omary, M. B. (1993). A significant soluble keratin fraction in 'simple' epithelial cells. Lack of an apparent phosphorylation and glycosylation role in keratin solubility. *J. Cell Sci.* **105**, 433-444.

Colakoglu, G. and Brown, A. (2009). Intermediate filaments exchange subunits along their length and elongate by end-to-end annealing. *J. Cell Biol.* **185**, 769-777.

Dross, N., Spriet, C., Zwerger, M., Muller, G., Waldeck, W. and Langowski, J. (2009). Mapping eGFP oligomer mobility in living cell nuclei. *PLoS One* **4**, e5041.

Ellenberg, J., Siggia, E. D., Moreira, J. E., Smith, C. L., Presley, J. F., Worman, H. J. and Lippincott-Schwartz, J. (1997). Nuclear membrane dynamics and reassembly in living cells: targeting of an inner nuclear membrane protein in interphase and mitosis. *J. Cell Biol.* **138**, 1193-1206.

Goldman, R. D., Grin, B., Mendez, M. G. and Kuczmarski, E. R. (2008). Intermediate filaments: versatile building blocks of cell structure. *Curr. Opin. Cell Biol.* **20**, 28-34.

Helfand, B. T., Chang, L. and Goldman, R. D. (2004). Intermediate filaments are dynamic and motile elements of cellular architecture. *J. Cell Sci.* **117**, 133-141.

Herrmann, H., Bar, H., Kreplak, L., Strelkov, S. V. and Aebi, U. (2007). Intermediate filaments: from cell architecture to nanomechanics. *Nat. Rev. Mol. Cell Biol.* **8**, 562-573.

Jaitovich, A., Mehta, S., Na, N., Ciechanover, A., Goldman, R. D. and Ridge, K. M. (2008). Ubiquitin-proteasome-mediated degradation of keratin intermediate filaments in mechanically stimulated A549 cells. *J. Biol. Chem.* **283**, 25348-25355.

Kim, S. and Coulombe, P. A. (2007). Intermediate filament scaffolds fulfill mechanical, organizational, and signaling functions in the cytoplasm. *Genes Dev.* **21**, 1581-1597.

Kirmse, R., Portet, S., Mucke, N., Aebi, U., Herrmann, H. and Langowski, J. (2007). A quantitative kinetic model for the in vitro assembly of intermediate filaments from tetrameric vimentin. *J. Biol. Chem.* **282**, 18563-18572.

Kolsch, A., Windoffer, R. and Leube, R. E. (2009). Actin-dependent dynamics of keratin filament precursors. *Cell Motil. Cytoskeleton* **66**, 976-985.

Kreis, S., Schonfeld, H. J., Melchior, C., Steiner, B. and Kieffer, N. (2005). The intermediate filament protein vimentin binds specifically to a recombinant integrin alpha2/beta1 cytoplasmic tail complex and co-localizes with native alpha2/beta1 in endothelial cell focal adhesions. *Exp. Cell Res.* **305**, 110-121.

Ku, N. O. and Omary, M. B. (2000). Keratins turn over by ubiquitination in a phosphorylation-modulated fashion. *J. Cell Biol.* **149**, 547-552.

Lee, C. H. and Coulombe, P. A. (2009). Self-organization of keratin intermediate filaments into cross-linked networks. *J. Cell Biol.* **186**, 409-421.

Listwan, P. and Rothnagel, J. A. (2004). Keratin bundling proteins. *Methods Cell Biol.* **78**, 817-827.

Magin, T. M., Vijayaraj, P. and Leube, R. E. (2007). Structural and regulatory functions of keratins. *Exp. Cell Res.* **313**, 2021-2032.

Margolis, R. L. and Wilson, L. (1981). Microtubule treadmills-possible molecular machinery. *Nature* **293**, 705-711.

Miller, R. K., Vikstrom, K. and Goldman, R. D. (1991). Keratin incorporation into intermediate filament networks is a rapid process. *J. Cell Biol.* **113**, 843-855.

Nikolic, B., Mac Nulty, E., Mir, B. and Wiche, G. (1996). Basic amino acid residue cluster within nuclear targeting sequence motif is essential for cytoplasmic plectin-vimentin network junctions. *J. Cell Biol.* **134**, 1455-1467.

Omary, M. B., Ku, N. O., Liao, J. and Price, D. (1998). Keratin modifications and solubility properties in epithelial cells and in vitro. *Subcell. Biochem.* **31**, 105-140.

Patterson, G. H. and Lippincott-Schwartz, J. (2002). A photoactivatable GFP for selective photolabeling of proteins and cells. *Science* **297**, 1873-1877.

Pekny, M. and Lane, E. B. (2007). Intermediate filaments and stress. *Exp. Cell Res.* **313**, 2244-2254.

Pollard, T. D., Blanchoin, L. and Mullins, R. D. (2000). Molecular mechanisms controlling actin filament dynamics in nonmuscle cells. *Annu. Rev. Biophys. Biomol. Struct.* **29**, 545-576.

Sivaramakrishnan, S., DeGiulio, J. V., Lorand, L., Goldman, R. D. and Ridge, K. M. (2008). Micromechanical properties of keratin intermediate filament networks. *Proc. Natl. Acad. Sci. USA* **105**, 889-894.

Small, J. V. and Resch, G. P. (2005). The comings and goings of actin: coupling protrusion and retraction in cell motility. *Curr. Opin. Cell Biol.* **17**, 517-523.

Soellner, P., Quinlan, R. A. and Franke, W. W. (1985). Identification of a distinct soluble subunit of an intermediate filament protein: tetrameric vimentin from living cells. *Proc. Natl. Acad. Sci. USA* **82**, 7929-7933.

Spurny, R., Gregor, M., Castanon, M. J. and Wiche, G. (2008). Plectin deficiency affects precursor formation and dynamics of vimentin networks. *Exp. Cell Res.* **314**, 3570-3580.

Steinbock, F. A., Nikolic, B., Coulombe, P. A., Fuchs, E., Traub, P. and Wiche, G. (2000). Dose-dependent linkage, assembly inhibition and disassembly of vimentin and cytokeratin 5/14 filaments through plectin's intermediate filament-binding domain. *J. Cell Sci.* **113**, 483-491.

Strnad, P., Windoffer, R. and Leube, R. E. (2002). Induction of rapid and reversible cytokeratin filament network remodeling by inhibition of tyrosine phosphatases. *J. Cell Sci.* **115**, 4133-4148.

Sun, N., Critchley, D. R., Paulin, D., Li, Z. and Robson, R. M. (2008a). Human alpha-synemin interacts directly with vinculin and metavinculin. *Biochem. J.* **409**, 657-667.

Sun, N., Critchley, D. R., Paulin, D., Li, Z. and Robson, R. M. (2008b). Identification of a repeated domain within mammalian alpha-synemin that interacts directly with talin. *Exp. Cell Res.* **314**, 1839-1849.

Tsuruta, D. and Jones, J. C. (2003). The vimentin cytoskeleton regulates focal contact size and adhesion of endothelial cells subjected to shear stress. *J. Cell Sci.* **116**, 4977-4984.

Vijayaraj, P., Sohl, G. and Magin, T. M. (2007). Keratin transgenic and knockout mice: functional analysis and validation of disease-causing mutations. *Methods Mol. Biol.* **360**, 203-251.

Wilkie, K. P. and Vrscay, E. R. (2005). Mutual information-based methods to improve local region-of-interest image registration. In *Image Analysis and Recognition* (*Lecture Notes in Computer Science*), Vol. 3656 (ed. M. Kamel and A. Campilho), pp. 63-72. Berlin/Heidelberg: Springer.

Windoffer, R. and Leube, R. E. (2001). De novo formation of cytokeratin filament networks originates from the cell cortex in A-431 cells. *Cell Motil. Cytoskeleton* **50**, 33-44.

Windoffer, R. and Leube, R. E. (2004). Imaging of keratin dynamics during the cell cycle and in response to phosphatase inhibition. *Methods Cell Biol.* **78**, 321-352.

Windoffer, R., Beile, B., Leibold, A., Thomas, S., Wilhelm, U. and Leube, R. E. (2000). Visualization of gap junction mobility in living cells. *Cell Tissue Res.* **299**, 347-362.

Windoffer, R., Woll, S., Strnad, P. and Leube, R. E. (2004). Identification of novel principles of keratin filament network turnover in living cells. *Mol. Biol. Cell* **15**, 2436-2448.

Windoffer, R., Kolsch, A., Woll, S. and Leube, R. E. (2006). Focal adhesions are hotspots for keratin filament precursor formation. *J. Cell Biol.* **173**, 341-348.

Woll, S., Windoffer, R. and Leube, R. E. (2005). Dissection of keratin dynamics: different contributions of the actin and microtubule systems. *Eur. J. Cell Biol.* **84**, 311-328.

Woll, S., Windoffer, R. and Leube, R. E. (2007). p38 MAPK-dependent shaping of the keratin cytoskeleton in cultured cells. *J. Cell Biol.* **177**, 795-807.

Würflinger, T., Bergmeister, M., Böcking, A., Meyer-Ebrecht, D. and Aach, T. (2008). Image registration for multimodal cell analysis. *Cell. Oncol.* **30**, 166.

Yoon, K. H., Yoon, M., Moir, R. D., Khuon, S., Flitney, F. W. and Goldman, R. D. (2001). Insights into the dynamic properties of keratin intermediate filaments in living epithelial cells. *J. Cell Biol.* **153**, 503-516.

Zatloukal, K., French, S. W., Stumptner, C., Strnad, P., Harada, M., Toivola, D. M., Cadrin, M. and Omary, M. B. (2007). From Mallory to Mallory-Denk bodies: what, how and why? *Exp. Cell Res.* **313**, 2033-2049.